Single Crystal Structure and Opto-electronic Properties of Oxidized Spiro-OMeTAD

Wei Zhang,[a] Linqin Wang,[b] Yu Guo,[a] Biaobiao Zhang,[b] Valentina Leandri,[a] Bo Xu,[b] Zhuofeng Li,[a] James M. Gardner,[a] Licheng Sun,[b, c] and Lars Kloo[a*]

[a] Department of Chemistry, Applied Physical Chemistry, KTH Royal Institute of Technology, SE-10044 Stockholm, Sweden

[b] Department of Chemistry, Organic Chemistry, KTH Royal Institute of Technology, SE-10044 Stockholm, Sweden

[c] State Key Laboratory of Fine Chemicals, DUT-KTH Joint Research Center on Molecular Devices, Dalian University of Technology (DUT), 116024 Dalian, China

Corresponding author: larsa@kth.se

Experimental details

Materials

Chemicals and solvents were purchased from Sigma Aldrich and were used without further purification, except when explicitly mentioned below. Spiro-OMeTAD (99.8%) was purchased from Borun New Material. Poly(2,3-dihydrothieno-1,4-dioxin)-poly(styrenesulfonate) (PEDOT:PSS) (Al 4083) was purchased from Ossila.

Synthesis of Spiro(TFSI)$_2$.

Spiro(TFSI)$_2$ was synthesized according to previous instructions in the literature.[1] Briefly, Spiro-OMeTAD (574 mg) was dissolved in 60 mL degassed dichloromethane (DCM). Silver bis(trifluoromethanesulfonyl)imide (AgTFSI) (400 mg) was then added in one portion. The solution changes color immediately from pale yellow to dark red. The solution was stirred under an N$_2$ atmosphere at room temperature for 24 hours. Filtration to remove Ag particles, and the filtrate was subsequently concentrated by rotary evaporation and precipitated using diethyl ether, affording a dark green powder (792 mg, 95% yield). Elemental Analysis: Expected: C 57.17, H 3.84, F 12.77, N 4.71, S 7.18. Experiment: C 55.02, H 4.01, F 12.86, N 4.69, S 7.21. ^{19}F NMR: -78.57 ppm.

Crystallization of Spiro(TFSI)$_2$

Excess Spiro(TFSI)$_2$ was dissolved in DCM under stirring in a closed vial at room temperature, yielding a dark red solution. The solution was filtrated through a Millipore membrane (0.2 μm) filter using a syringe. The filtrated solution was stored in a small vial (5 mL), and was later transferred inside a big vial (20 mL) containing ethyl ether (8 mL), the solutions were thus not mixed. The outer vial was closed tightly, and the system was then transferred into a dark environment. The slow evaporation of the anti-solvent (ethyl ether) into the small vial containing the DCM solution of Spiro(TFSI)$_2$ triggered the crystallization and growth of single crystals suitable for X-ray diffraction analysis.

Hole mobility measurements

The hole mobility of the materials in this study was determined according to literature methods.[2, 3] Briefly, a hole-conducting-only device with the structure of FTO/PEDOT:PSS/HTM/Au was fabricated. The fluorine-doped tin-oxide (FTO) coated glass substrates (Pilkington TEC15) were etched with Zn powder and a 2 M HCl solution. The substrates were then sequentially washed with soap, acetone and alcohol by sonication for 30 minutes. The remaining organic residues were removed with using a plasma cleaner (Harrick Plasma) for 30 min. A roughly 40 nm PEDOT:PSS layer was then spin-coated at 3000 rpm onto the substrate, followed by annealing at 120 °C for 20 min. A solution of 20 mM of Spiro(TFSI)$_2$ was then spin-coated on top of the annealed PEDOT:PSS layer, followed by evaporation of an 80 nm gold (Metalor; ≥99.99% trace metals basis) counter electrode. *J-V* characteristics of the devices were recorded with a Keithley 2400 Source-Meter unit, interfaced with a computer.

Conductivity measurements

The conductivity of the HTMs formed was investigated according to existing reports.[4, 5] Glass substrates without conductive layer were sequentially washed with soap, acetone, and alcohol by sonication for 30 minutes. A mesoporous TiO$_2$ layer was deposited by spin-coating at 3000 rpm for 30 s using a solution of 30 nm TiO$_2$ paste (Dyesol DSL 30NR-T) in absolute ethanol (w/w=1/3). After spin-coating, the substrate was immediately placed on a hotplate at 80 °C for 15 min, and then transferred to an oven and sintered at 500 °C for 30 min. 20 mM of Spiro(TFSI)$_2$ was subsequently spin-coated onto the mesoporous TiO$_2$ layer, followed by evaporation of 80 nm gold as counter electrode. *J-V* characteristics were recorded in the dark with a Keithley 2400 Source-Meter unit, interfaced with a computer.

Computational details

The molecular structures of Spiro-OMeTAD and Spiro(TFSI)$_2$ were either obtained from corresponding single crystal data or optimized in vacuum without any symmetry constrains, using density-functional theory (DFT) based on the hybrid cam-B3LYP functional and 6-31G** basis sets for all atoms. All reported molecular calculations were carried out by means of Gaussian 16.[6] Band structure calculations were performed using the Crystal17 program.[7] The cam-B3LYP functional was used together with basis sets for all atoms of 2-31G quality as provided by the program package. The calculations were based on the crystal structures. The crystal structure of Spiro-OMeTAD is straightforward to use as input for the band structure calculations.[8] However the crystal structure of Spiro(TFSI)$_2$ is complicated by a severe disorder of the TFSI$^-$ anion. Unfortunately, the disorder is linked to more than one symmetry element in the unit cell of the Fddd (70) space group, and thus the only solution to offer a unit cell suitable for calculation was to reduce symmetry to P1 (1) and thus remove the effects of anion disorder. The resulting model embraces 1528 atoms and 5592 atom orbitals, which represents a tremendeous calculational challenge solved by using OpenMPI over 32 processor cores.[9]

Characterization methods

Elemental analysis was performed by Analytische Laboratorien in Germany. Nuclear magnetic resonance (NMR) spectra were recorded on a Bruker AVANCE 400 MHz spectrometer. The powder X-ray diffraction data were recorded on a PANalytical-X'Pert PRO diffractometer using Cu-Kα radiation. The scanning electron microscopy (SEM) images were recorded on a FEI-XL 30 series microscope. Electron paramagnetic resonance (EPR) spectra were recorded under ambient condition on a Bruker EMX-micro spectrometer equipped with an EMX-Primium bridge and an ER4119HS resonator. Spiro(TFSI)$_2$ solutions were prepared in degassed acetonitrile with a concentration of 0.3 mM and loaded to capillary sample tubes (50 µl with one end open). The sample capillary was sealed using an EPR sealant after sample loading and was inserted into an EPR probe (i.d. 3 mm) for further examination. Cyclic voltammetry (CV) was performed in DCM solution with 0.1 M Tetrabutylammonium hexafluorophosphate ([TBA]PF$_6$) as supporting electrolyte, an Ag/AgNO$_3$ electrode as reference, a glassy carbon electrode as working electrode, a Pt rod as counter electrode and ferrocene/ferrocenium (Fc/Fc$^+$) as an internal reference using a CH Instruments electrochemical workstation (model 660 A). The CV scan rate used was 0.1 V/s. The electrolysis on Spiro-OMeTAD was performed in DCM solution with 0.1 M [TBA](PF$_6$) as supporting electrolyte, an Ag/AgCl electrode as reference, two Pt rods as electrodes. The UV/visible absorption spectra were recorded in acetonitrile solution on a PerkinElmer Lambda 750 spectrophotometer using a 1 cm thick cuvette. The single-crystal diffraction was detected using a Bruker D8 VENTURE diffractometer at room temperature operating with Mo Kα radiation. All structures were refined using SHELX.[10]

Scheme S1. Synthetic route for Spiro(TFSI)$_2$.
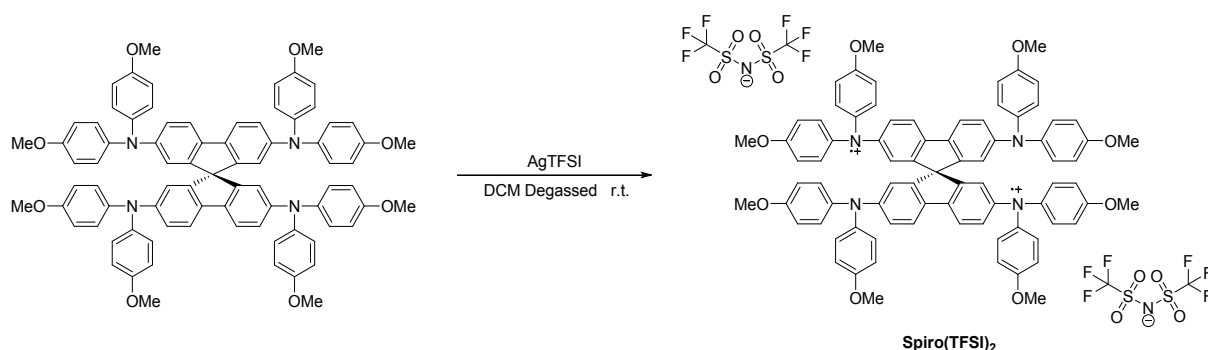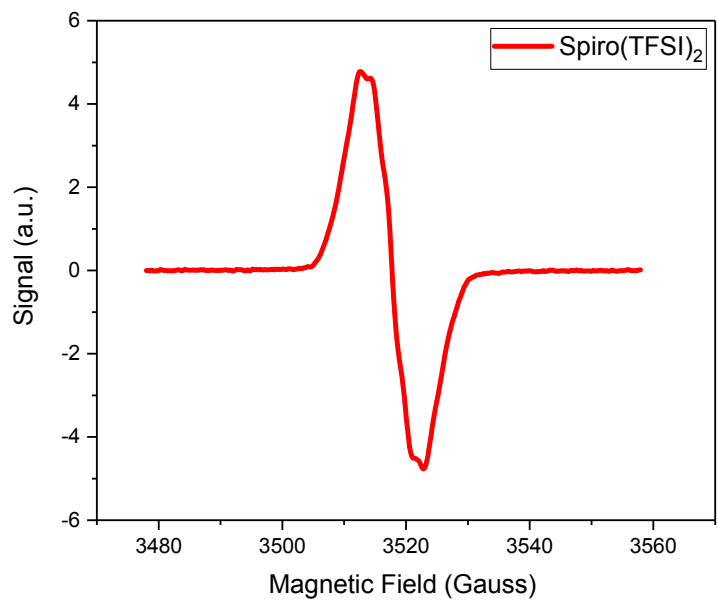
Fig. S1 EPR spectrum of Spiro(TFSI)$_2$ in acetonitrile.
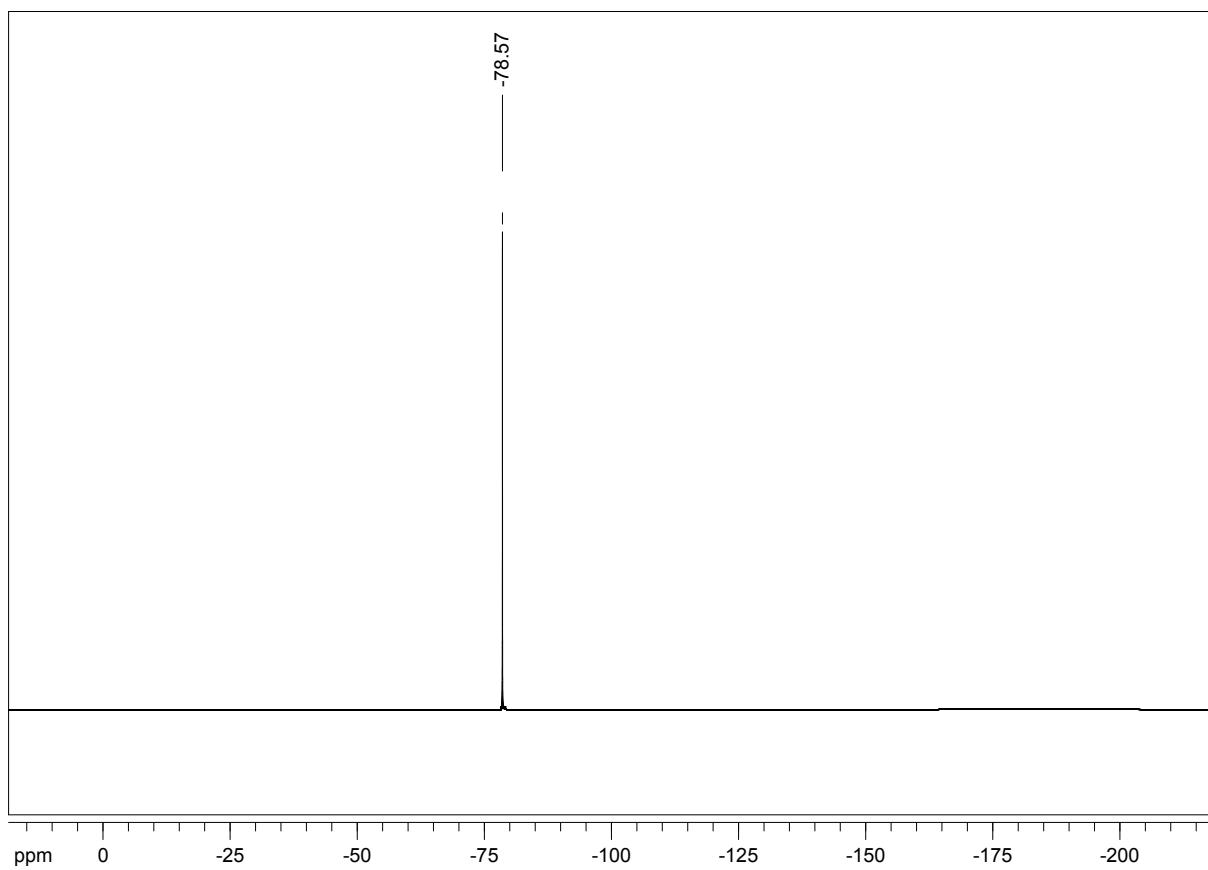
Fig. S2 ^{19}F NMR spectrum of Spiro(TFSI)$_2$ in DMSO-d6.

Table S1. Crystallographic data for Spiro(TFSI)$_2$

Molecular formula	$C_{85}H_{68}F_{12}N_6O_{16}S_4$
Formula weight (g/mol)	1785.72
Space group	Fddd (No. 70)
a (Å)	20.6770(4)
b (Å)	21.7260(4)
c (Å)	36.8774(7)
α (deg)	90
β (deg)	90
γ (deg)	90
V (Å^3)	16566(6)
Z	8
T (K)	293(2)
D$_{caled}$ (g cm^{-3})	1.432
R	0.0697 (3867)
wR2	0.2277
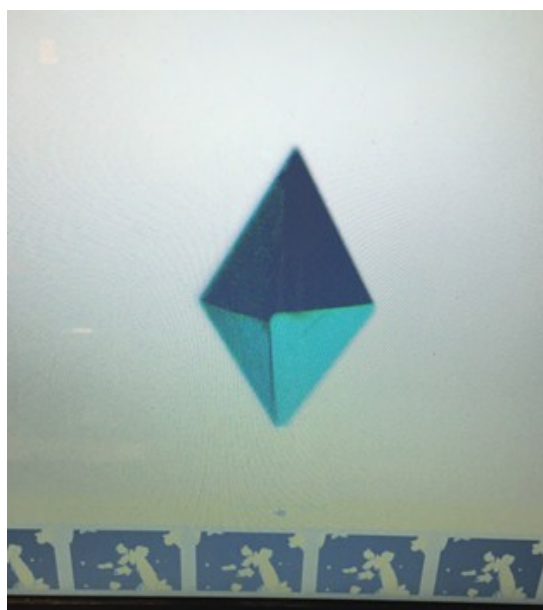
Fig. S3 Optical image of a Spiro(TFSI)$_2$ single crystal.
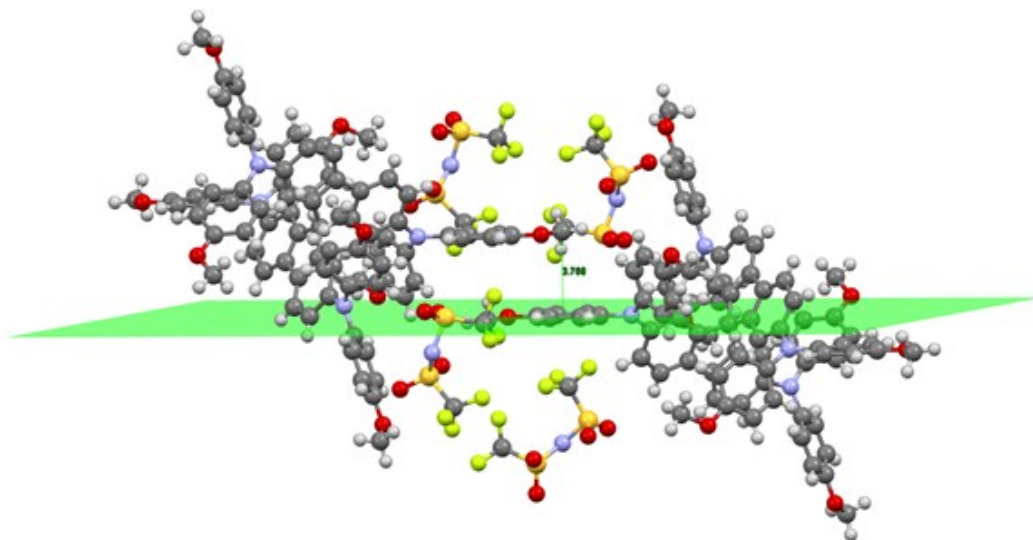
Fig. S4 Closest dimer in Spiro(TFSI)$_2$, as obtained from single-crystal diffraction.
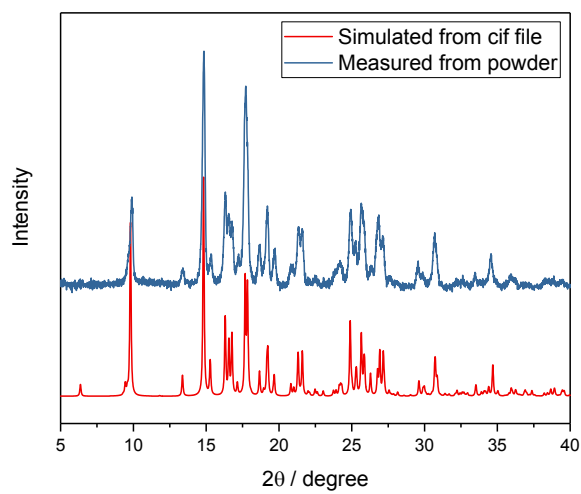
Fig. S5 The powder XRD pattern of Spiro(TFSI)$_2$ and a simulated pattern from single-crystal data.

Table S2. Unit cell parameters of Spiro(TFSI)$_2$.

Space group	a / Å	b / Å	c / Å	α / º	β / º	γ / º
Fddd (70)	20.6770(4)	21.7260(4)	36.8774(7)	90	90	90
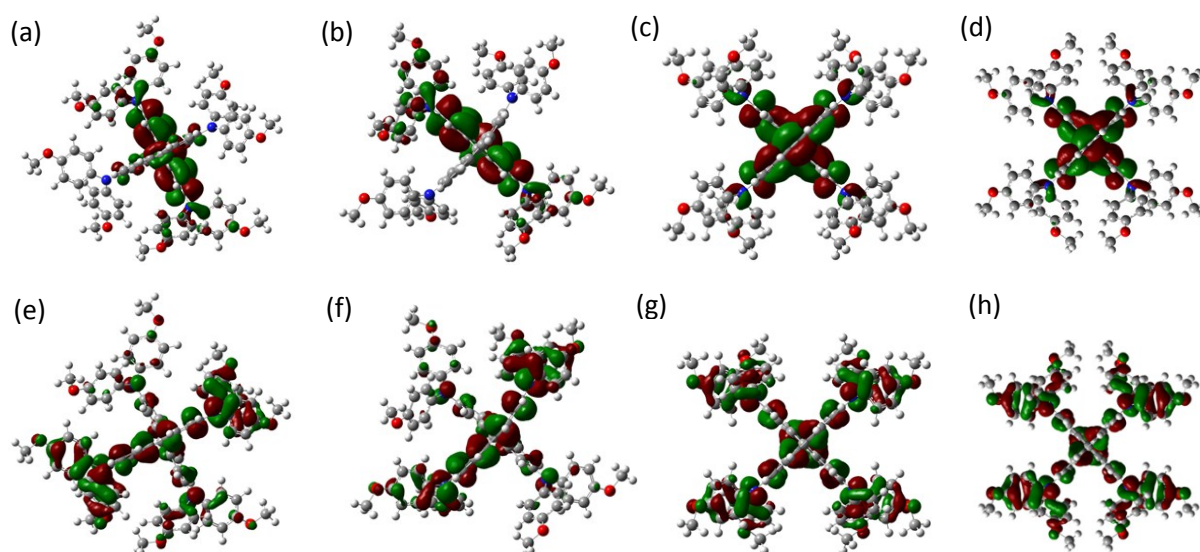
Fig. S6 LUMOs of (a) calculated Spiro-OMeTAD structure, (b) experimental Spiro-OMeTAD structure, (c) calculated Spiro^{2+} structure, (d) experimental Spiro^{2+} structure; HOMOs of (e) calculated Spiro-OMeTAD structure, (f) experimental Spiro-OMeTAD structure, (g) calculated Spiro^{2+} structure, (h) experimental Spiro^{2+} structure.

Table S3. Energy of frontier orbitals in Spiro-OMeTAD and Spiro^{2+}.

	Spiro-optimized / eV	Spiro-crystalized / eV	Spiro^{2+}-optimized / eV	Spiro^{2+}-crystalized / eV
LUMO+2	+0.90	+0.95	-3.56	-3.64
LUMO+1	+0.57	+0.84	-4.07	-4.11
LUMO	+0.56	+0.75	-4.09	-4.18
HOMO	-5.45	-5.35	-9.87	-9.90
HOMO-1	-5.48	-5.39	-9.89	-9.92
HOMO-2	-5.94	-6.00	-10.37	-10.32
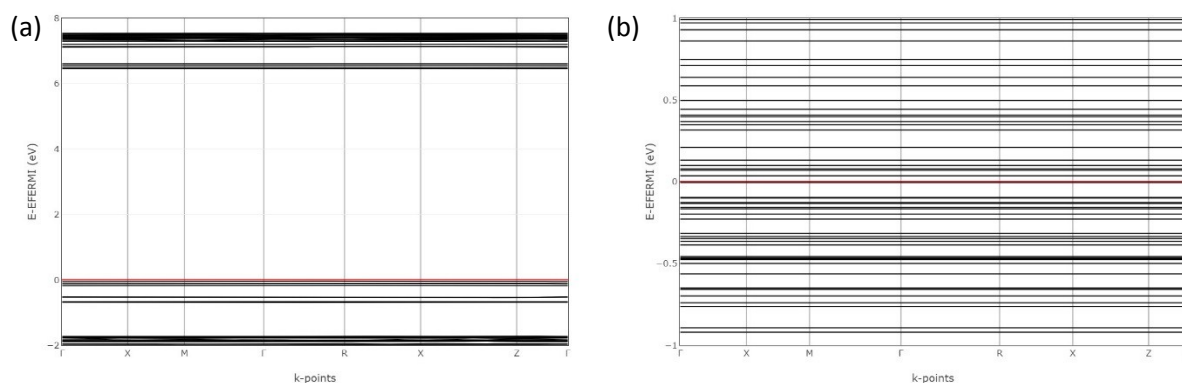
Fig. S7 Electronic band structure of (a) Spiro-OMeTAD; (b) Spiro(TFSI)$_2$. The crystallographic coordinates of high-symmetry points in the first Brillouin zone correspond to $\Gamma = (0,0,0)$, $X = (0.5,0,0)$, $M = (0.5,0.5,0)$, $R=(0.5,0.5,0.5)$, $Z= (0,0,0.5)$. The large bandgap of Spiro-OMeTAD conceals the fine structure of the valence band orbitals.
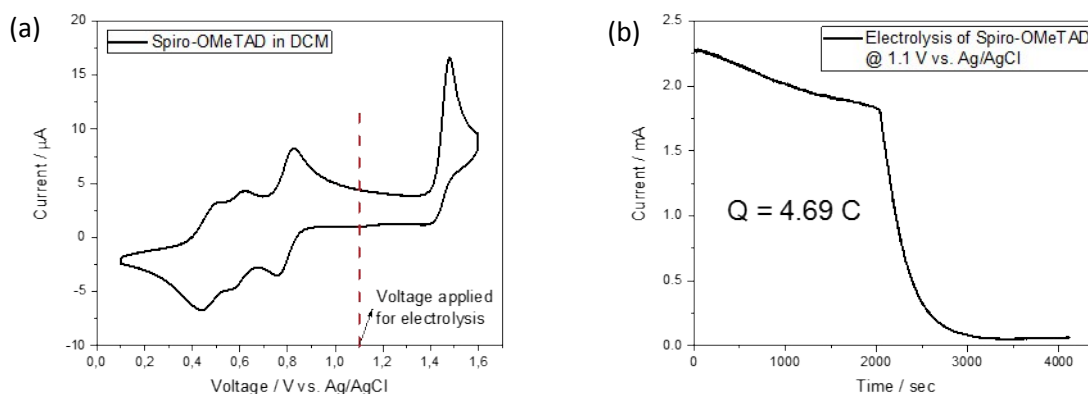
Fig. S8 (a) CV of Spiro-OMeTAD in DCM at high voltage, the voltage is given vs. Ag/AgCl. (b) Electrolysis of 15 mg Spiro-OMeTAD at a voltage of 1.1 V vs. Ag/AgCl. The charge collected is 4.69 C after 4000 seconds.

The estimate used to confirm our assignments is given below. The basic assumption is that if four electrons are lost by Spiro-OMeTAD below 1.1 V, the charge should be as follows,

$$Q = \frac{\frac{m}{M_w} \times N_0 \times 4 \times 1.602 \times 10^{-19}\, C}{}$$

$$= \frac{15 \times 10^{-3}}{1225.4} \times 6.022 \times 10^{23} \times 4 \times 1.602 \times 10^{-19}\, C$$

= 4.72 C

The calculated charge is quite similar to the one obtained (4.69 C) from the electrolysis experiment, indicating that four electrons are lost at an applied voltage 1.1 V vs. Ag/AgCl. This applied voltage is higher than the third peak but lower than the fourth oxidation peak. The electrolysis experiment consequently confirms our assignment that the third peak refers to a process $Spiro^{2+}$ to $Spiro^{4+}$, which is a two electron process.

Table S4. Optical properties of Spiro-OMeTAD and Spiro(TFSI)$_2$.

	Absorption wavelength / nm	Molar extinction coefficient / cm^{-1}/M
Spiro-OMeTAD	377	7.53×10^4
	371	1.74×10^4
	521	3.52×10^4
Spiro(TFSI)$_2$	691	8.91×10^3
	908	3.14×10^3
	1527	3.74×10^4
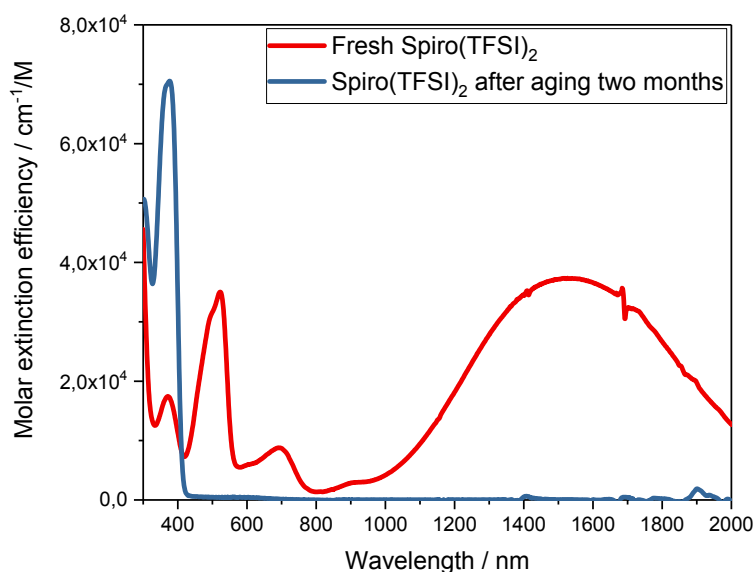
Fig. S9 UV/Visible absorption spectra of Spiro(TFSI)$_2$ as a fresh solution and after aging in acetonitrile (10^{-5} M) for two months.
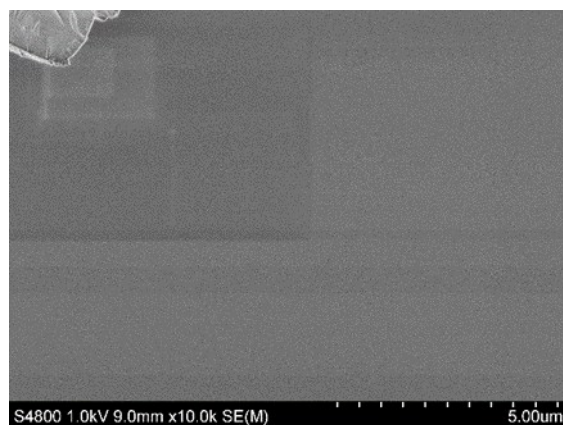
Fig. S10 SEM image of Spiro(TFSI)$_2$ film on top of PEDOT:PSS. The feature in the left-top corner is a glass cullet formed during sample preparation and was used for beam focusing. The square next to it is caused by beam damage due to the relatively low conductivity of the organic films.

References

1.   W. H. Nguyen, C. D. Bailie, E. L. Unger and M. D. McGehee, *J Am Chem Soc*, 2014, **136**, 10996-11001.
2.   C. Goh, R. J. Kline, M. D. McGehee, E. N. Kadnikova and J. M. J. Fréchet, *Applied Physics Letters*, 2005, **86**, 122110.
3.   I.-K. D. Tomas Leijtens, Tommaso Giovenzana, Jason T. Bloking, Michael D. McGehee, and Alan Sellinger, *ACS Nano*, 2012, **6**, 1455-1462.
4.   H. J. Snaith and M. Grätzel, *Applied Physics Letters*, 2006, **89**, 262114.
5.   H. J. Snaith and M. Grätzel, *Advanced Materials*, 2007, **19**, 3643-3647.
6.   M. J. Frisch, G. W. Trucks, H. B. Schlegel, G. E. Scuseria, M. A. Robb, J. R. Cheeseman, G. Scalmani, V. Barone, G. A. Petersson, H. Nakatsuji, X. Li, M. Caricato, A. V. Marenich, J. Bloino, B. G. Janesko, R. Gomperts, B. Mennucci, H. P. Hratchian, J. V. Ortiz, A. F. Izmaylov, J. L. Sonnenberg, Williams, F. Ding, F. Lipparini, F. Egidi, J. Goings, B. Peng, A. Petrone, T. Henderson, D. Ranasinghe, V. G. Zakrzewski, J. Gao, N. Rega, G. Zheng, W. Liang, M. Hada, M. Ehara, K. Toyota, R. Fukuda, J. Hasegawa, M. Ishida, T. Nakajima, Y. Honda, O. Kitao, H. Nakai, T. Vreven, K. Throssell, J. A. Montgomery Jr., J. E. Peralta, F. Ogliaro, M. J. Bearpark, J. J. Heyd, E. N. Brothers, K. N. Kudin, V. N. Staroverov, T. A. Keith, R. Kobayashi, J. Normand, K. Raghavachari, A. P. Rendell, J. C. Burant, S. S. Iyengar, J. Tomasi, M. Cossi, J. M. Millam, M. Klene, C. Adamo, R. Cammi, J. W. Ochterski, R. L. Martin, K. Morokuma, O. Farkas, J. B. Foresman and D. J. Fox, *Journal*, 2016.
7.   A. E. R. Dovesi, R. Orlando, C. M. Zicovich-Wilson, B. Civalleri, L. Maschio, M. Rerat, S. Casassa, J. Baima, S. Salustro, B. Kirtman., *WIREs Comput Mol Sci.*, 2018, **8**, e1360.
8.   D. Shi, X. Qin, Y. Li, Y. He, C. Zhong, J. Pan, H. Dong, W. Xu, T. Li, W. Hu, J.-L. Brédas and O. M. Bakr, *Science Advances*, 2016, **2**, e1501491.
9.   T. o. s. c. b. o. f. t. w. N. https://www.open-mpi.org/.
10.   G. Sheldrick, *Acta Crystallographica Section A*, 2008, **64**, 112-122.